Chapter 4

Numerical experiments

As described in section 3.2, two sets of numerical experiments will be carried out. In the first set the temperature structure will be simulated using estimation of vertical velocity (section 4.1), and in the second set vertical velocity will be simulated using observed temperature profile (section 4.2).

4.1 Temperature structure simulations

Several simulations are carried out to examine the role of the various processes controlling the upper-ocean thermal structure during October 1994 to October 1995 in the central Arabian Sea. Several estimates of the advective heat fluxes will be used. The plan for the experiments is as follows:

Experiment-1: Role of local atmospheric forcing fluxes from Weller et al. [2] (simulation S1).

Experiment-2: Advective heat fluxes based on Fischer et al. [4] is added to S1. This experiment is further divided into two parts.

- (i) Addition of Fischer-based horizontal advection (S2a).
  (Forcing: Atmospheric fluxes + Horizontal advection)
- (ii) Addition of Fischer-based vertical advection (S2b).
  (Forcing: Atmospheric fluxes + Horizontal advection + Vertical advection)

Experiment-3: Advective heat fluxes based on optimally interpolated data (Reynolds [103]) and on the SODA OGCM added to experiment S1. This experiment is further divided into two parts.

- (i) Addition of horizontal advection (S3a)
  (Forcing: Atmospheric fluxes + Horizontal advection).

- (ii) Addition of vertical advections (S3b)

  (Forcing: Atmospheric fluxes + Horizontal advection + Vertical advection).

4.1.1 Role of local surface fluxes (simulation S1)

In the first simulation (S1), only the local atmospheric (surface) forcing fluxes are taken into account. These fluxes (Weller et al. [2]) were described in section 3.1.1. These fluxes are dominated by the monsoonal cycle. During the NE monsoon, the ocean surface is subjected to a moderate wind forcing. During the SW monsoon, the ocean surface is subjected to a strong wind forcing and gains heat. During the IMs, the ocean surface is subjected to a weak wind forcing and is continuously heated up by the increasing solar radiation. It is thus expected that SST will decrease and ML will deepen during the NE monsoon owing to convective entrainment driven by net heat loss at the surface, whereas deepening of ML and decrease of SST are expected during the SW monsoon owing to mixing driven by strong winds. Continuous increase of SST and a shallow ML are expected during the IMs owing to strong insolation and reduced nonsolar heat fluxes and wind forcing.

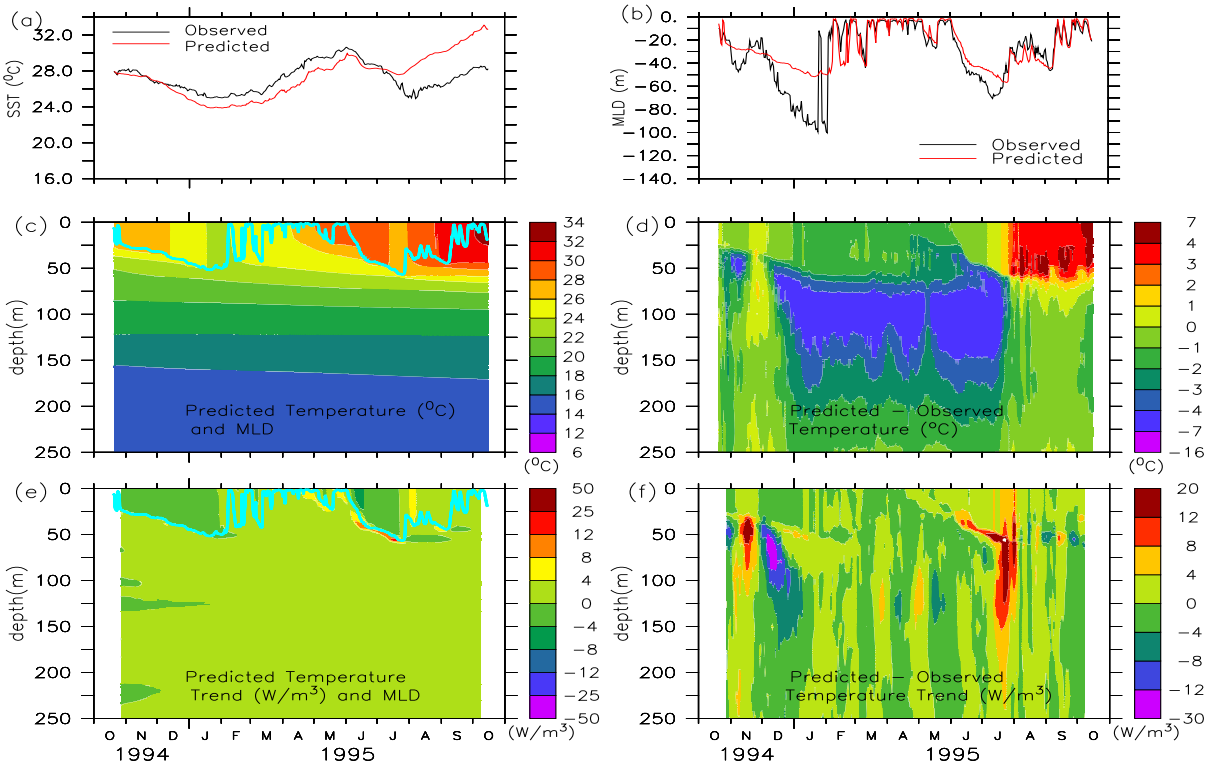

Figure 4.1: Results of the numerical simulation S1 (forcing by atmospheric fluxes): (a) predicted (red) and observed (black) SST; (b) predicted (red) and observed (black) MLD; (c) vertical structure of temperature (color) and MLD (blue line); (d) predicted minus observed temperature; (e) vertical structure of predicted temperature trend (color) and MLD (blue line); (f) predicted minus observed temperature trend. The data in the figure are smoothed with low pass filters: two hours for SST (a); one day for MLD (b), and for temperature profiles (c) and (d); 10 days for the trends of temperature profile (e) and (f).

The results of the (S1) simulation are compared to the observations in Fig. 4.1. As expected, the predicted SST follows an annual cycle similar to that observed (Fig. 4.1a). There are, however, significant differences between them. The predicted SST diverges from the observations during December. The model remains too cool (by 1 °C) until the beginning of the SW monsoon. Then it becomes increasingly too warm (by up to 5-6 °C at the end of the run). The general trends in the predicted MLD are similar to those in the observed MLD throughout the year (see Fig. 4.12). However, significant differences occur, as in the case of SST. In particular, the transient change (meso-scale feature) in November 1994 is not reproduced and the deepening during the NE monsoon is strongly underestimated (50 m predicted in January vs 100 m in the observations). From the end of the NE monsoon the model MLD almost parallels the observations, except for the meso-scale feature in August. Evolution of the predicted vertical temperature profile (Fig. 4.1) shows

that the impact of the surface forcing fluxes does not penetrate deeper than the predicted MLD. The difference between the predicted and the observed temperature is shown in Fig. 4.1d. As expected from the SST behaviour, the temperature predicted for the near surface layer remains close to the observation from the beginning of the study period to the middle of the SW monsoon. After that, the model warms up too much. In contrast, the sub-surface layer is poorly simulated until the middle of the SW monsoon (with a maximum underestimate of 6 °C). As regards the temperature trend (see Fig. 4.1e), none of the sub-surface warming and cooling events are reproduced. As a consequence, the differences between the predicted and observed temperature trends (see Fig. 4.1f) during the monsoonal period are large (more than 4 W m^{-3}), and mostly equal and opposite to the observed trends (see Fig. 3.3c). The difference is not so significant (less than 4 W m^{-3}) during January–June (Spring IM), which suggests that the sub-surface temperature underestimates during the IM (Fig. 4.1d) mostly resulted from the earlier (December) underestimate.

In summary, this simulation shows that the atmospheric forcing explains only the general trend of near-surface layer thermal structure (evolution of SST and MLD). It alone is unable to explain the annual evolution of the whole upper layer. This implies that the role of other (oceanic) processes must be taken into account.

4.1.2 Forcing with Fischer-based estimates of heat advection

4.1.2.1 Forcing: atmospheric flux + Fischer-based horizontal advection (S2a)

In this experiment, in addition to local atmospheric surface forcing (same as in S1), the influence of horizontal advection is also taken into account. These fluxes were, due to Fischer et al. [4] described in section 3.2.3. These fluxes are associated with strong episodic warming and cooling events (strength up to 80 W m^{-3}) during both the monsoons in the sub-surface layers, which are much stronger than the warming and cooling trends present in the observed temperature field (see Fig. 3.3c).

The results (S2a) are compared with the observations in Fig 4.2. The predicted SST rapidly diverges from the observed values from the beginning of the study period (Fig.4.2a). The bias increases up to -6 °C at the end of December as a consequence of strong cooling (15 W m^{-3}, near the surface) by advection. The difference remains more or less constant until the end of the study period. As regards the MLD evolution (see Fig. 4.2b), its deepening is too slow from the beginning of the study period until early December as compared to the observations. After that, the MLD almost coincides with the observations for the rest of the year. The agreement between the predicted MLD of this simulation and the observed MLD is better than for S1.

The predicted evolution of the vertical temperature profile (Fig. 4.2c) shows that the horizontal advection of heat strongly affects the temperature evolution. The sub-surface temperature cools down to 16 °C at 40 m depth during the NE monsoon, and down to 12 °C below 60 m during the SW monsoon. As shown in Fig. 4.2d, the difference between predicted and observed temperature is very large (upto -7 °C) for the whole domain. The excess cooling that occurred during early November within the upper 80 m gradually penetrates the whole vertical domain during the rest of the period, and by the end of July it covers the entire vertical domain (0–250 m). In contrast, the excess warming that occurred in the lower part of the model domain below 80 m during the same period gradually decays and by mid-July, it almost disappears. The predicted temperature trend and the difference between the trends in predicted and observed temperatures are presented in Fig. 4.2. As seen in Fig. 4.2e, unlike in the previous simulation S1, the warming and cooling trends are reproduced in the sub-surface layers, but with significant bias. The predicted trend has huge amplitudes (up to 30 W m^{-3}) from 20 October to mid-November and August to early September. The predicted trend is overestimated significantly during late November to early December (up to 12 W m^{-3}) and then during the end of the simulation (early October 1995; up to 20 W m^{-3}). Outside of these two periods, the difference is not so significant (less than 8 W m^{-3}).

In summary, this simulation S2a (Fig. 4.2) shows that the period from 20 October to mid-November 1994 is the most critical. The excess cooling caused by the horizontal advective heat fluxes during this period in the upper 80 m affects the whole simulation. The horizontal advective heat estimates used during this period are probably responsible for this bias.

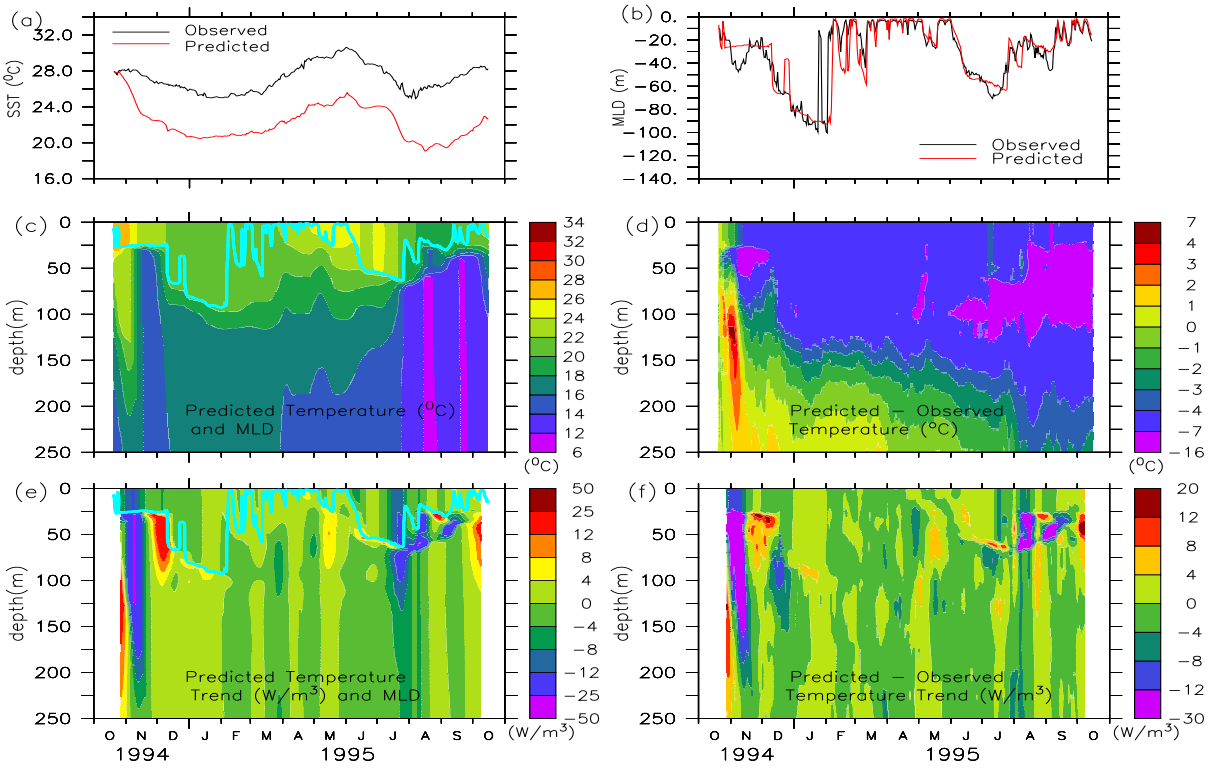

Figure 4.2: Results of the numerical simulation S2a : (a) predicted (red) and observed (black) SST; (b) predicted (red) and observed (black) MLD; (c) vertical structure of temperature (color) and MLD (blue line); (d) predicted minus observed temperature; (e) vertical structure of predicted temperature trend (color) and MLD (blue line); (f) predicted minus observed temperature trend. The data are smoothed as in Fig. 4.1.

4.1.2.2 Forcing: atmospheric fluxes + Fischer-based horizontal advection + Fischer-based vertical advection (S2b)

As described in section 3.2.6.2 Fischer et al. [4] estimated the heat conserving vertical velocity at the study location at 125 m. The same estimate is used to construct the vertical velocity profile for 0-250 m layer using the method described in section 3.2.6.2. These estimates are used to force the model in addition to atmospheric fluxes and horizontal advective heat fluxes. The simulated (S2b) temperature structure is presented in the Fig. 4.3. The results are mostly similar to S2a and clearly show that these vertical velocity estimates are unable to improve the vertical temperature structure obtained with S2a simulation.

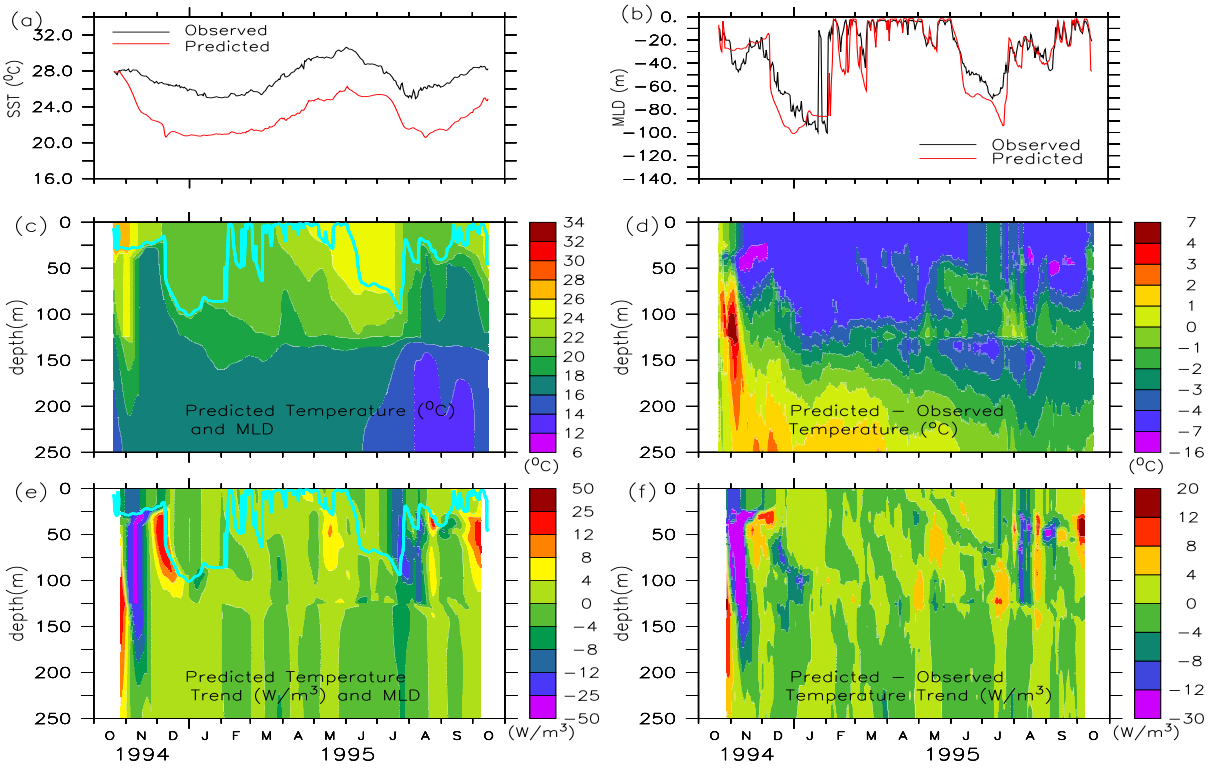

Figure 4.3: Results of the numerical simulation S2b : (a) predicted (red) and observed (black) SST; (b) predicted (red) and observed (black) MLD; (c) vertical structure of temperature (color) and MLD (blue line); (d) predicted minus observed temperature; (e) vertical structure of predicted temperature trend (color) and MLD (blue line); (f) predicted minus observed temperature trend. The data are smoothed as in Fig. 4.1.

4.1.3 Experiments with present study estimates of advective heat fluxes

In the above, the *in-situ* estimates of the horizontal advective heat fluxes based on Fischer et al. [4] were used to examine their role in predicting the temperature structure. These advective heat fluxes are associated with large uncertainties (Fischer et al. [4]) and they did not allow a proper simulation of the temperature evolution. Alternative and independent estimates of the horizontal advective heat fluxes and vertical velocity are therefore required (see section 3.2.5 and 3.2.6), and such estimates are now used to force the model.

4.1.3.1 Forcing: atmospheric flux + Reynolds-based horizontal advection (S3a)

The model is forced with the measured advective heat fluxes based on Reynolds temperature gradient (see section 3.2.5) together with atmospheric fluxes. The results of the simulated temperature structure are presented in Fig. 4.4. As seen in Fig 4.4a, the predicted SST is lower than observed through most of the year, but the agreement is much better than S2a throughout the year and bet-

ter than S1 after the onset of the SW monsoon. From mid-October to mid-November, the cooler waters advected from the northwest (Figs. 3.12c-d) lead to a 1°C underestimate, which is partially compensated by the arrival of warmer waters from the southeast in December. The strongest advection impact occurs during the SW monsoon, due to cooler waters advected first from the west and then from the northwest. This allows the model to remain relatively close to the observations. As regards the MLD evolution (Fig. 4.4b), the main difference with S1 is the increase in the NE monsoon deepening by (up to 60 m in January vs 50 m in S1). Evolution of the vertical profile (Fig. 4.4c) shows that horizontal advection of heat (see Figs. 3.12d) also has an impact on sub-surface variability. As shown in Fig. 4.4d, the difference between model and data is similar to that for S1, except for a slight decrease in the mid-November to mid-December overestimate and for the significant improvement in the surface layer after early July. It is nevertheless worth noting that at sub-surface levels, the model diverges more than does S1 in early November and from August to October. The predicted temperature trend (Fig. 4.4e) and the difference between the predicted and observed temperature trend (Fig. 4.4f) are almost similar to S1.

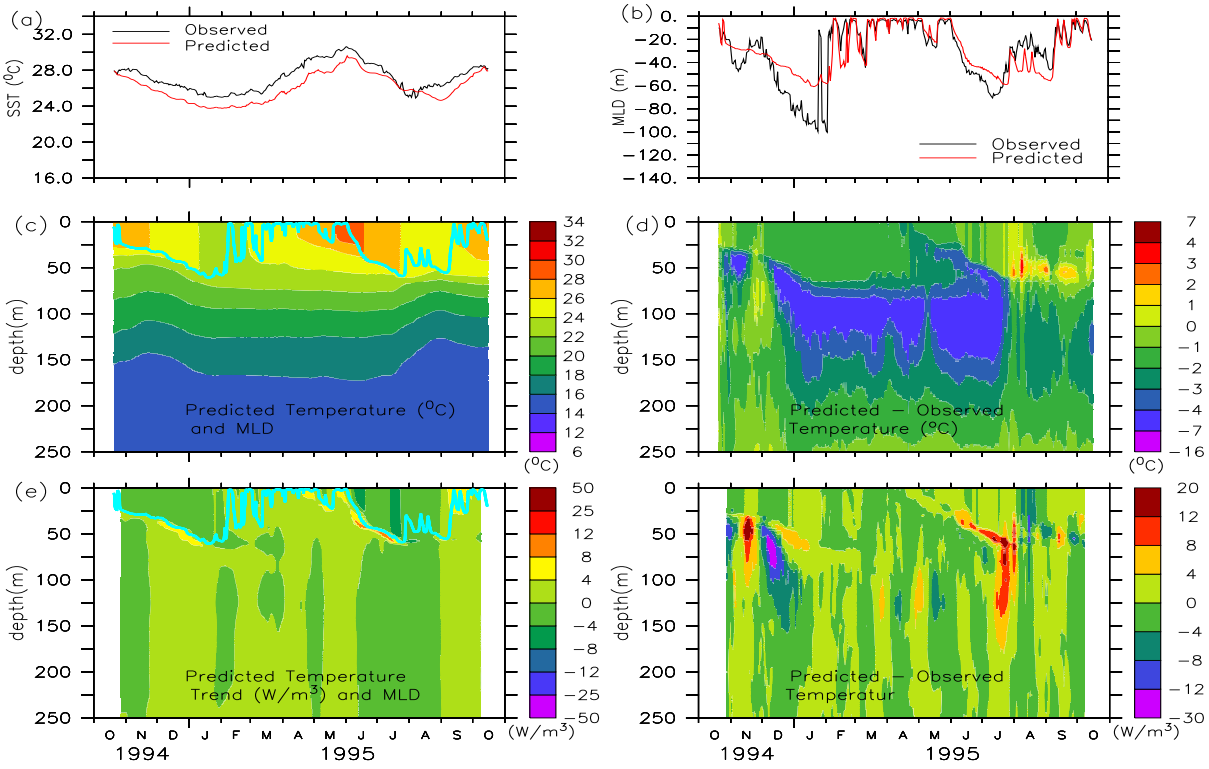

Figure 4.4: Results of the numerical simulation S3a: (a) predicted (red) and observed (black) SST; (b) predicted (red) and observed (black) MLD; (c) vertical structure of predicted temperature (color) and MLD (blue line); (d) modeled minus observed temperature; (e) vertical structure of predicted temperature trend (color) and MLD (blue line); (f) predicted minus observed temperature trend. The data are smoothed as in Fig. 4.1.

4.1.3.2 Forcing: atmospheric fluxes + Reynolds-based horizontal advection + SODA-OGCM-based vertical advection (S3b)

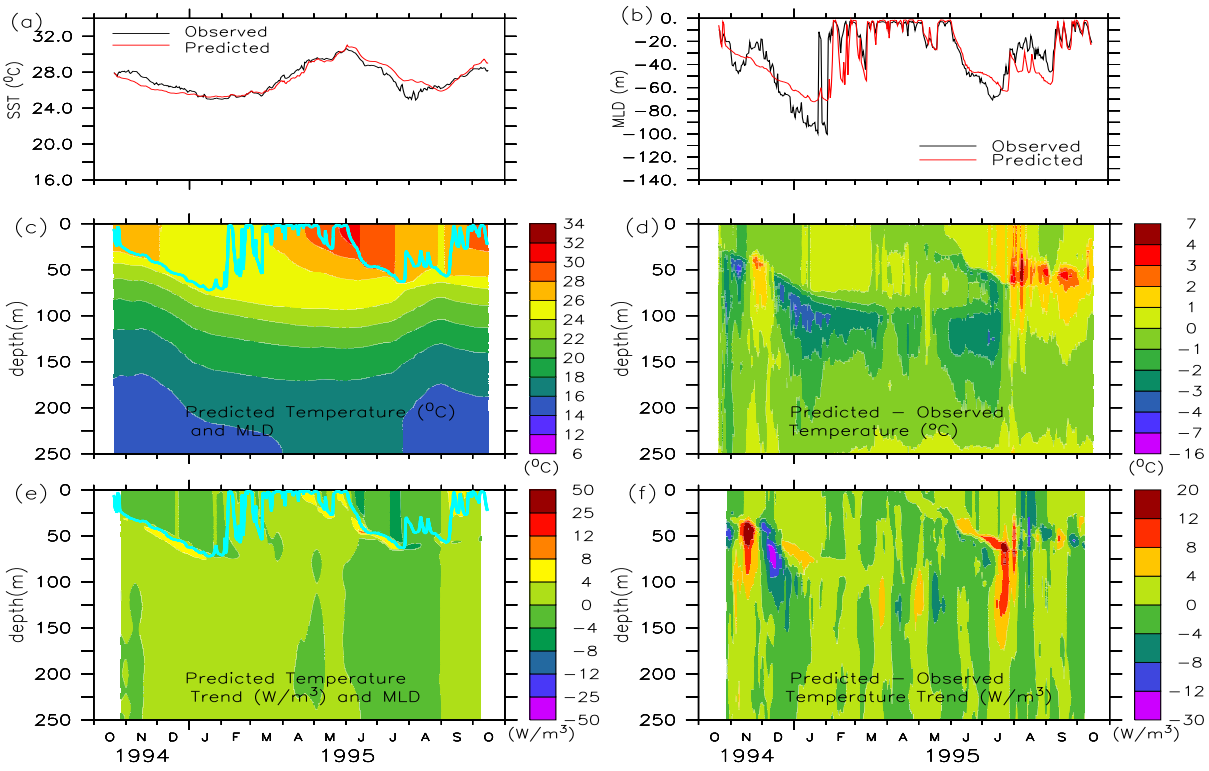

Figure 4.5: Results of the numerical simulation S3b: (a) predicted (red) and observed (black) SST; (b) predicted (red) and observed (black) MLD; (c) vertical structure of predicted temperature (color) and MLD (blue line); (d) modeled minus observed temperature; (e) vertical structure of predicted temperature trend (color) and MLD (blue line); (f) predicted minus observed temperature trend. The data are smoothed as in Fig. 4.1.

To include the impact of vertical advection, only the data of vertical velocity are required as the model uses its own predicted temperature gradient. The data of vertical velocity for this simulation are based on SODA OGCM (see section 3.2.6). In this experiment (S3b), when the combined effect from horizontal and vertical advection are considered, the temperature structure is reproduced well (see Fig 4.13), and is significantly better than earlier simulations (S3a, S2b, and S1). The predicted SST (Fig. 4.13a) remains close to the observations all through the year, except for an underestimate from mid-October to the end of November (1 °C at the most) and for an overestimate between late July and late August (2 °C at the most). As regards the MLD evolution (Fig. 4.13b), the main improvement is the increase in the NE monsoon deepening (now up to 75 m in January). The observed intra-seasonal variations in temperature vertical structure are better reproduced by the model (see Fig. 4.13c); there is considerable improvement in particular at sub-surface

levels. This is a consequence of warm surface water down-welled to the sub-surface during the NE monsoon and weak upwelling of cool water from the deeper ocean to the sub-surface (see Fig. 3.13). The differences between the simulated and the observed temperatures remain small in the near-surface layer all along the year, except for a departure of ~2 °C from late July to mid-August (Fig. 4.13d). At sub-surface levels, significant departures from the observations are still present in a rather narrow depth interval at the base of the ML. Over the year the mean temperature in the mixed layer differs from the observed mean by +0.02 °C and the temperature profiles are simulated with an accuracy of 1.86 ± 1.57 % (mean ± standard deviation) in terms of absolute relative error, while the mean temperature difference is -0.41 °C and the accuracy is (-2.0 ± .05 %) for the 0 – 250 m layer.

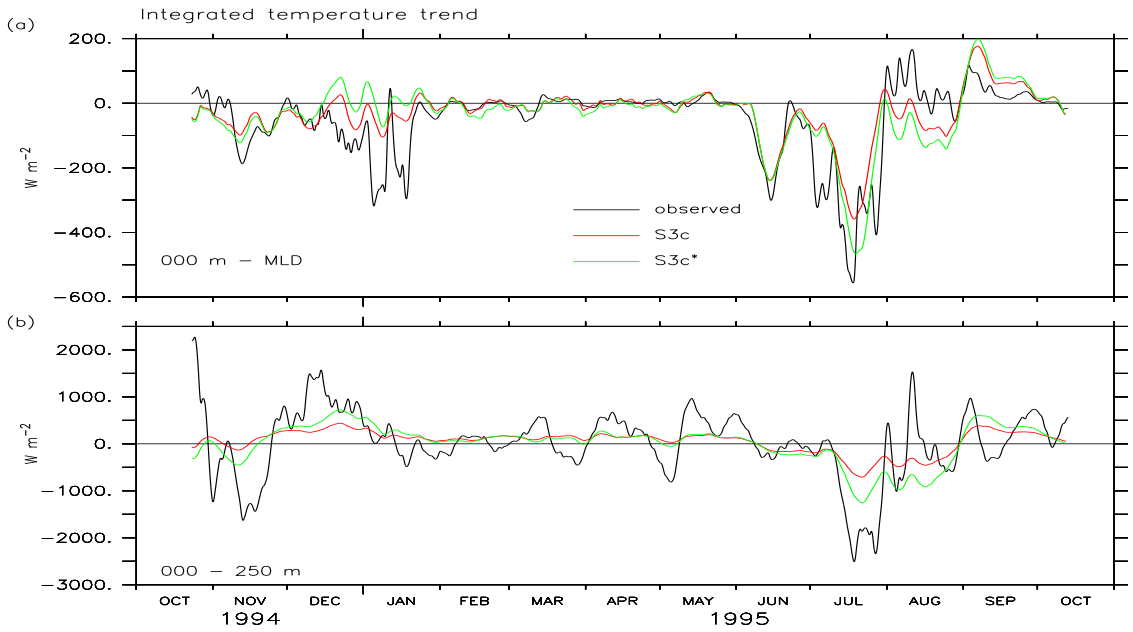

Figure 4.6: (a) Evolution of the observed (black) and the predicted temperature trend integrated over the ML and (b) over the 0–250 m layer (lower panel) for simulations S3b (red) and for S3b* (green) (see text in section4.1.4.4 for simulation S3b*).

The trend in the predicted temperature is integrated over the ML and over the 0–250 m layer and is compared to the observed trend in Figs. 4.6 (in units of heat flux). As shown (upper panel), this simulation could reproduce most of the observed features in terms of magnitude as well as variability for the ML. For the whole simulated layer (lower panel), the variability of main seasonal features are reproduced, but with significantly underestimated amplitude. The short term events (several days to several weeks) are missing.

This result shows the simulation S3b improved considerably from the S2b estimate, but this improvement is, however, not enough as most of small scale events are missing in S3b in the sub-surface (see Figs. 4.6). There are two causes for this: (i) the estimates of horizontal advective fluxes used in the simulation is not proper in the sub-surface, and (ii) the SODA vertical velocity does not contain such variability.

4.1.4 Discussion

4.1.4.1 Sensitivity to atmospheric forcing fluxes

The surface forcing fluxes used in all the above simulations were computed from measurements at the mooring (Weller et al. [2]) at high resolution. It is important to know how sensitive are the model results to possible inaccuracies of atmospheric forcing fluxes. Therefore, a number of sensitivity experiments have been carried out with respect to various atmospheric fluxes in Appendix B.3. Results of the experiments suggest that the predicted SST and MLD do not change significantly for a 10% change in the strength of wind stress: MLD changes by upto 4 m and SST changes by upto 0.2^{o}C month^{-1} during the SW monsoon only. However, they are highly sensitive to 10% change in either surface-heat gain through solar radiation or loss through long-wave radiation and through turbulent fluxes of latent heat and sensible heat (change is upto 1 ^{o}C month^{-1} in SST and change in MLD is upto 10 m). The experiment also shows that the predicted temperature structure is the best when the model is forced with the estimated values published by Weller et al. [3].

4.1.4.2 What causes the most general trends in SST and MLD evolution ?

According to Weller et al. [3] and Fischer et al. [4], the general trend of the SST and MLD during the NE monsoon (cooling of SST and deepening of MLD) is due to convective entrainment-mixing driven by buoyancy (heat) loss at the surface, whereas the trend of the MLD and SST during the SW monsoon (deepening of ML and cooling of SST) is due to turbulent mixing driven by wind stress. The earlier study by McCreary et al. [83] suggests that there is significant role of buoyancy-driven mixing in deepening of MLD and in cooling of SST in northern Arabian Sea during the SW monsoon. Sensitivity experiments are carried out with respect to various surface fluxes in Appendix B.3.3. The results of the simulations agree with the conclusion made by Weller et al. [3] and Fischer et al. [4] for the NE monsoon, but not for the SW monsoon. The experiments show that the deepening of MLD during the SW monsoon cannot be explained by wind stress

alone. A significant contribution comes from the buoyancy-driven convective entrainment mixing (in particular during June–July).

4.1.4.3 Fischer-based horizontal advection

The estimates of horizontal advective heat fluxes from Fischer et al. [4] were available only for 0–125 m. These estimates have been used to construct the advective heat fluxes for upper 250 m (see section 3.2.3) ($A(z)$) assuming that the horizontal temperature gradient remains uniform below 125 m. The constructed horizontal advective heat fluxes $A(z)$ are used in S2a (S2b) simulation to predict the temperature evolution. In order to examine the validity of the assumption, the above construction $A(z)$ can be replaced by alternative data constructions by relaxing our assumptions of uniform temperature gradient below 125 m. Two other constructions were considered. Heat flux $A(z)$ was changed according to a 50% decrease and increase in the temperature gradient between 125 m and 250 m depths. Sensitivity experiments show model simulation S2a and S2b remain unchanged. The results of simulations S2a and S2b suggest that Fischer-based horizontal advective heat fluxes are highly biased in the upper 80 m during the early NE monsoon (from 20 October to mid-November 1994) and are responsible for large misestimates of the predicted thermal structure during subsequent periods. Another simulation is carried out by initialising the model on 15 November (instead of 20 October) (see S2a* simulation in Appendix D.1). The simulation confirmed that the enormous cooling driven by horizontal advection of the near-surface layer during the early NE monsoon dominates the model prediction during the rest of the year. Thus this cooling signal in the horizontal advective heat estimates is suspect. During the rest of the year, the estimates of horizontal heat fluxes may be considered good.

The Fischer-based horizontal advective heat fluxes were estimated by using the observed horizontal currents at the central mooring and the horizontal temperature gradient estimated from the three (out of four) associated corner moorings (see Fig. 1.3). These advective heat fluxes are associated with strong signals of warming and cooling events and over most of the year these estimates are under the uncertainly level (Fischer et al. [4]). Temperature structure obtained from the four moorings, north-west mooring (NWM), south-west mooring (SWM), south-east mooring (SEM), and central mooring (CM) (see Fig. F.1 in Appendix F), suggest that the temperature structure from the south-west mooring differs significantly from the temperature structure obtained from the rest of the moorings during November (difference in mean temperature of 50–100 m layer is upto 4^{o}C) and during August (upto 3^{o}C). According to Weller et al. [3], and Fischer et al. [4], satellite altimeter data imagery shows that meso-scale eddies passed through the mooring array during the

early NE monsoon (November) and late SW monsoon (August). The temperature structures from these mooring shows that the south-east mooring reflects strongly this signature, whereas other moorings are less (negligibly) affected by the meso-scale system. Hence Fischer-based horizontal advective heat fluxes might be not representative for the central mooring.

4.1.4.4 Reynolds-based horizontal advection

The second set of horizontal advective heat fluxes (Reynolds-based) used in simulation S3b (S3a) does a significantly better job than the Fischer-based estimates. However, as these estimates are derived from interpolated satellite temperature (see section 3.2.5) combined with in situ current measurements, they suffer from scale inconsistency. Another drawback of these estimates is the assumption that the temperature gradient remains constant over the entire depth range (0–250 m). This assumption is not likely to be perfect. How sensitive is the temperature simulation to horizontal temperature gradient variations with depth ?

To address the issue, another simulation S3b* similar to S3b, is carried out by varying the horizontal advection in the sub-surface layers. The gradient increases to twice its surface value at 80 m and reduces to the surface value at 200 m and remains constant (as the surface value) below. This choice is based on the variability of sub-surface temperature from SODA and from Levitus [29]. The results of the new simulation (S3b*) are expressed in the form of integrated temperature trend over the ML and over the 0–250 m layer, and compared to the earlier results of S3b in Figure 4.6. The results show that the integrated trend over the ML (for the S3b* simulation) is slightly improved during July, but still deviate from the observations during December and August. This implies that the correction in the horizontal advective heat fluxes for the ML is not necessary. Regarding the whole layer, the integrated trend improved significantly during the NE monsoon and during July of the SW monsoon, but the amplitudes of the variations were still significantly weaker than the observations during most of the year.

4.1.5 Concluding remarks

The S1 simulation shows that the local atmospheric forcing fluxes mostly control the near-surface layer thermal structure during the year, but not during the SW monsoon. The near-surface layer thermal structure during the SW monsoon, and the sub-surface layer during most period of the year can not be explained through atmospheric forcing fluxes alone. Comparing S2b to S2a and S1, and S3b to S3a and S1 shows that horizontal advection is mainly responsible for the cooling of the near-surface layer during the SW monsoon.

Two sets of advective heat fluxes have been used to correct the temperature prediction. The prediction based on the first set show high-frequency signals associated with local scales. The prediction based on the second set is more representative of large scales. The vertical velocity estimates involved in the first set of advective correction is not independent of horizontal advection estimates as it is determined as a residual of the heat budget (see Section 3.2.3). The vertical velocity based on SODA-OGCM involved in the second set of advective correction is independent of horizontal advection but it has no high-frequency variability.

Among all the simulations carried out in this section, the SODA-based simulation (S3b) is the best, however, that is still far from the observed temperature structure: most of small-scale signals are underestimated. As there is no any better and independent estimates of vertical velocity available than the SODA-based estimate, we attempt the inverse approach: the model is used to predict the vertical velocity in the following section.

4.2 Prediction of the vertical velocity

The model is now used to predict the vertical velocity instead of predicting the temperature structure. For this, the model is forced with atmospheric fluxes and horizontal advective heat fluxes, together with observed temperature (see Fig. 3.9). The first estimate of vertical velocity will be derived in the case of Fischer-based horizontal advective heat fluxes and the second will be derived in the case of Reynolds-based horizontal advective heat fluxes. The computation technique (for both estimates) was described in section 3.2.6.2.

4.2.1 Estimates of vertical velocity: case of Fischer-based horizontal advection

The estimated vertical velocity is shown in Fig. 4.7 (contour). The associated estimates of vertical advection of heat (colour) is also shown. The estimated vertical velocity is large and structured during the monsoonal periods. In most of the cases the large values of vertical velocity coincides with the large horizontal advective heat fluxes used in the model simulation (see Fig. 3.10). Significant upwelling occurs during early October 1994 (8 m day^{-1}, in the lower domain, below 80 m), late November 1994 (3 m day^{-1}), and late August 1995 (3 m day^{-1}). Significant downwelling occurs (30 m day^{-1}) during October to mid-November 1994 in the upper domain (between surface to 120 m), December (3 m day^{-1}), and during late July to mid-August (10 m day^{-1} just below the ML and is around 3 m day^{-1} below 80 m). From early January to early July, weak vertical movements (mostly episodic, less than 1 m day^{-1}) prevail.

The part of the figure (domain) marked with a red circle (upper 80 m, during 20 October to mid-November 1994) is the most critical period: the corresponding estimated vertical velocity is unrealistically large (more than 30 m day^{-1}). It is worth noting that this huge (negative) amplitude of vertical velocity corresponds to the very large magnitude (strength 80 W m^{-3}) of the horizontal advective heat fluxes (see Fig. 3.10).

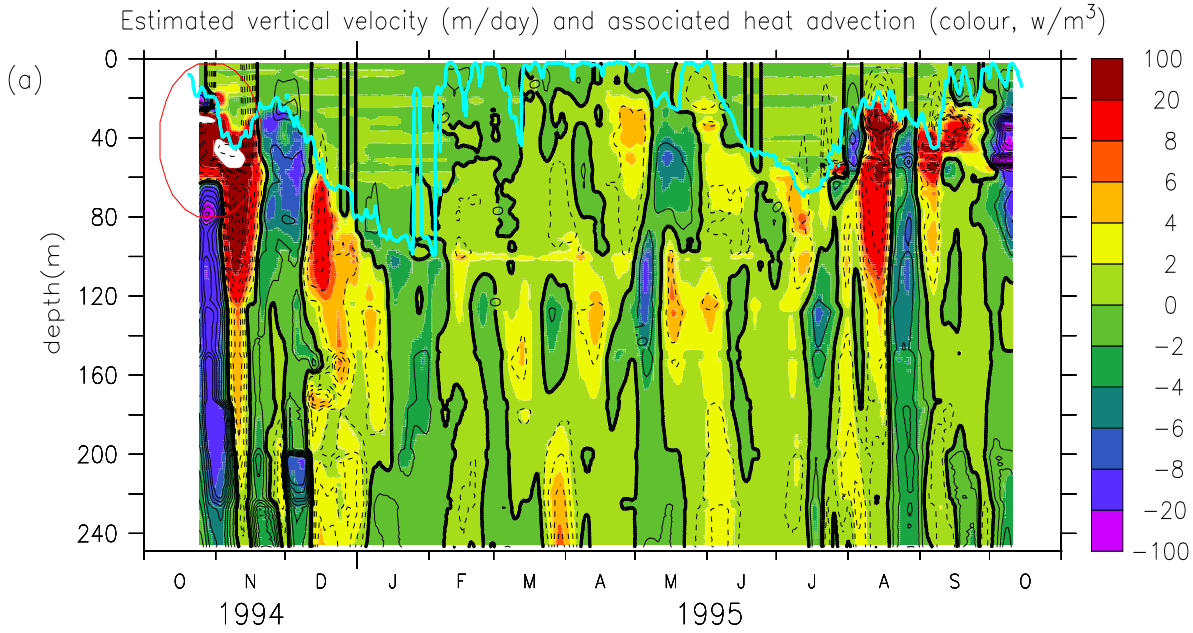

Figure 4.7: (a) Contours of vertical velocity (WFR, m day^{-1}) estimated in the present study. Thin solid lines represent positive velocities; dashed lines represent negative velocities; thick solid lines represent zero velocities. Contour interval: 1 m day^{-1}. Advective heat fluxes: colour, W m^{-3}. MLD: blue line. The red circle corresponds to very high values of WFR (see the text).

These estimated vertical velocities (WFR) at 125 m are compared with the heat-conserving vertical velocities (W_H) as estimated by Fischer et al. [4] in Fig. 4.8. During most of the year, strength of the model velocity WFR is weaker than the heat conserving velocity W_H. During late October 1994, WFR is large and positive (upto 8 m day^{-1}), in contrast to the huge and negative value of WFR (18 m day^{-1}). From early November to late December, both estimates show almost similar variation, with differences in amplitude of the variation. During the first half of January, WFR is negative with strength upto 2 m day^{-1} in contrast to the large positive values of W_H (-6 m day^{-1}). During the Spring IM, variation of WFR is mostly oscillating around zero with amplitude 1.5 m day^{-1} in contrast to mostly negative values of W_H strength upto 2 m day^{-1}. During early SW monsoon (June) both are negligible, and during the rest of the SW monsoon, WFR differs significantly from W_H except for a short duration in early August. The model velocity WFR is

positive during July and August (with strength upto 3 m day^{-1}), in contrast to negative values of W_H during the same periods (with strength upto 5m day^{-1} in July and 14 m day^{-1} in August). During the Autumn IM, WFR is negligible, in contrast to significant negative values of W_H (3 m day^{-1}).

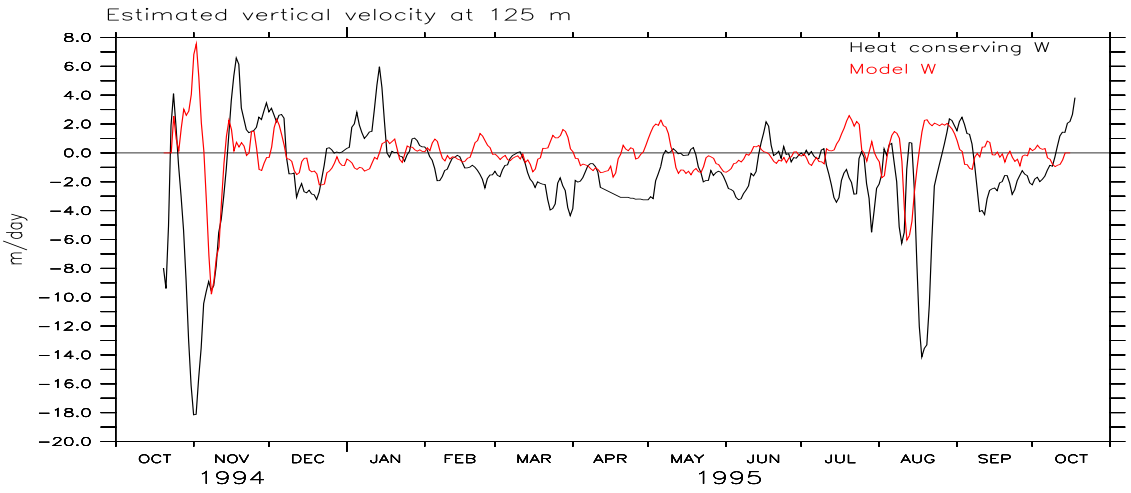

Figure 4.8: Comparison between the heat conserving vertical velocity as estimated by Fischer et al. [4] at 125 m and the model vertical velocity at 125 m.

4.2.1.1 Testing WFR: Temperature simulation with atmospheric fluxes, Fischer-based horizontal advection, and WFR (S2c)

Since we have estimated vertical velocity, these estimates need to be examined for their consistency. Therefore, simulation of temperature field is carried out by forcing the TKE model with the estimated vertical velocity (see Fig. 4.7a) to include the effect of vertical advection together with the corresponding estimates of horizontal advective heat fluxes and local air-sea fluxes (as used in S2a). The prediction is expected to match the observations. The results of the simulation (S2c) are presented in Fig. 4.9. The predicted temperature evolution, as inferred from the structure of predicted SST (Fig. 4.9a), MLD (Fig. 4.9b), temperature profile (Fig. 4.9c), and the difference between the predicted and the observed temperature structure (Fig. 4.9) is unsatisfactory. In contrast, the temperature trend (see Figs. 4.9d and 4.9e) is reproduced well except in the upper 80 m domain during the early NE monsoon (20 October - 15 November 1994). It is clear from Fig. (4.9e) that the actual problem lies within the ML in early NE monsoon. It is worth noting that even strong (strength upto 40 m day^{-1}) downwelling estimated in the ML and just below the ML during

this period is unable to produce sufficient warming to compensate the enormous cooling of about 20 W m^{-3} caused by horizontal advection. Our calculations suggest that the required estimates of vertical velocity should be larger than 250 m day^{-1} in order to compensate the same amount of cooling in the ML driven by horizontal advction.

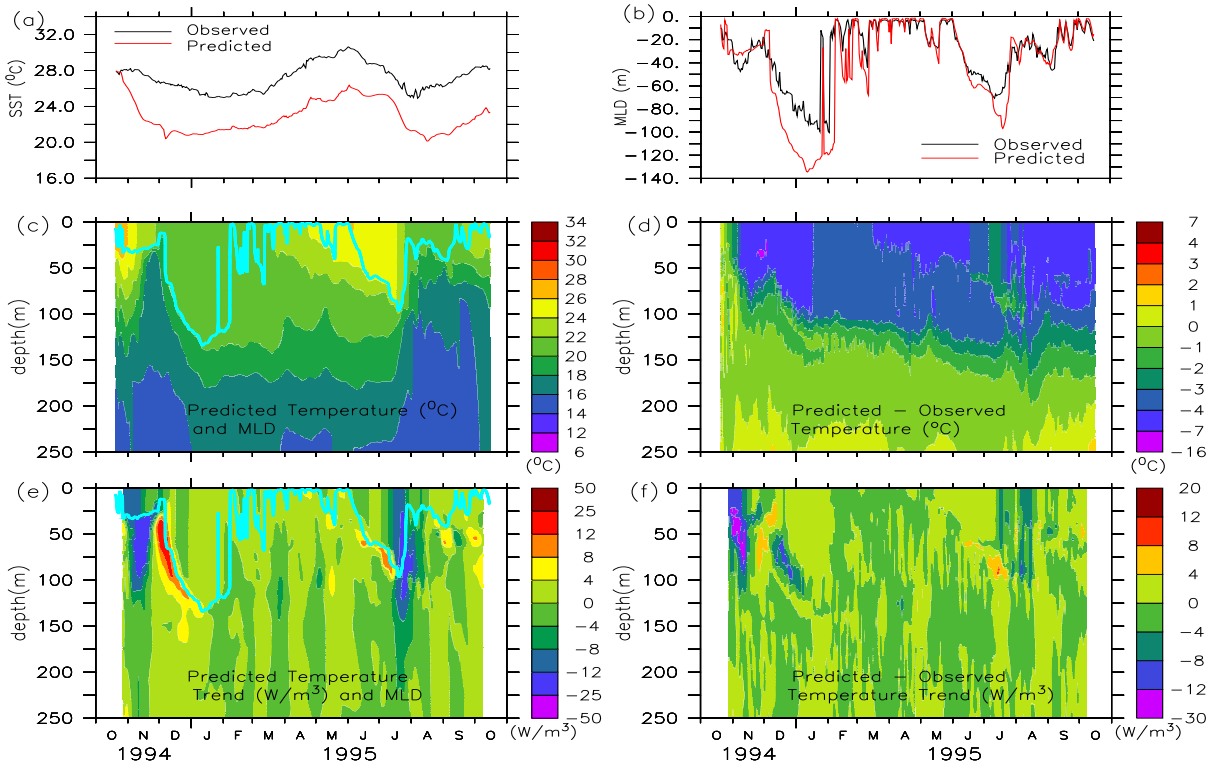

Figure 4.9: Results of the numerical simulation S2c: (a) predicted (red) and observed (black) SST; (b) predicted (red) and observed (black) MLD; (c) vertical structure of predicted temperature (color) and MLD (blue line); (d) modeled minus observed temperature; (e) vertical structure of predicted temperature trend (color) and MLD (blue line); (f) predicted minus observed temperature trend. The data are smoothed as in Fig. 4.1.

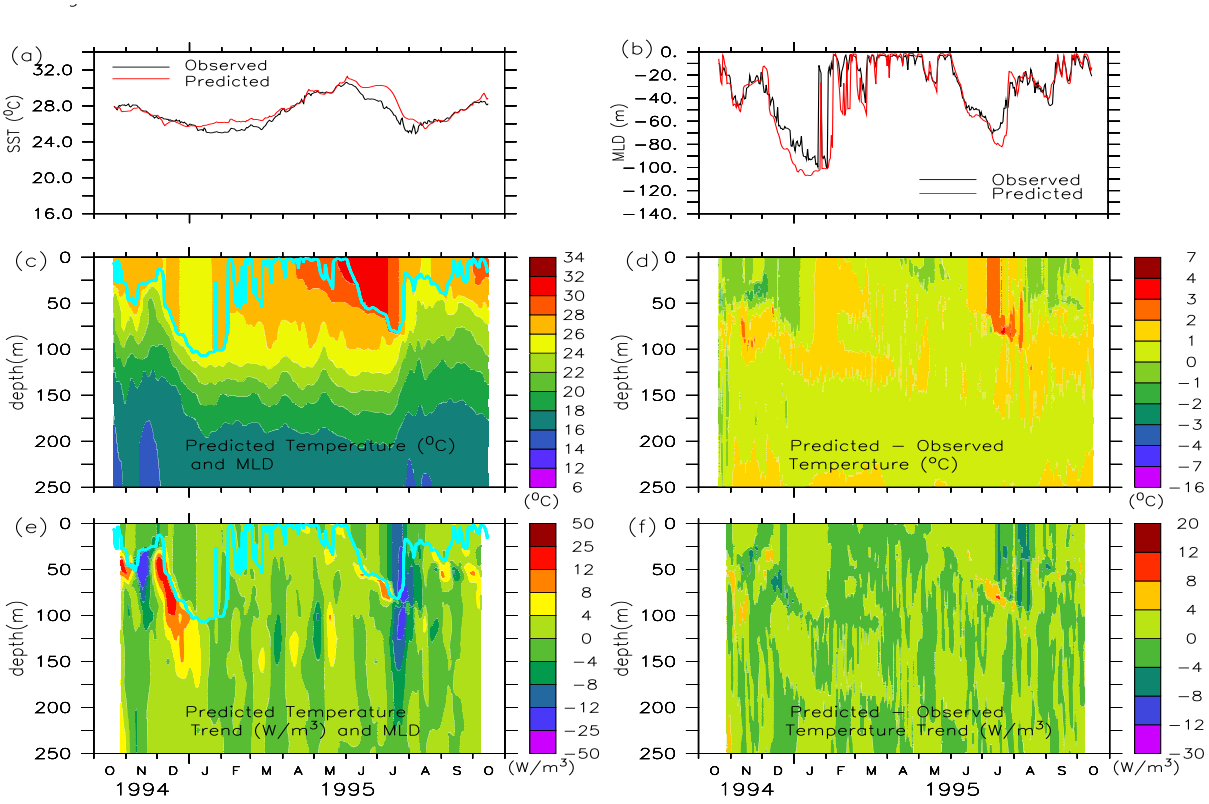

Figure 4.10: Results of the numerical simulation S2c*: (a) predicted (red) and observed (black) SST; (b) predicted (red) and observed (black) MLD; (c) vertical structure of predicted temperature (color) and MLD (blue line); (d) modeled minus observed temperature; (e) vertical structure of predicted temperature trend (color) and MLD (blue line); (f) predicted minus observed temperature trend. The data are smoothed as in Fig. 4.1.

An additional (S2c*) simulation is carried out by assuming a zero value for the horizontal advective heat flux within the ML during early NE monsoon. The predicted temperature structure matches the observation throughout the year at all depths. The predicted SST (Fig. 4.10a), MLD (Fig. 4.10b), vertical predicted temperature structure (Fig. 4.10c) and the predicted temperature trend (Fig. 4.10e) are reproduced well. This result is also seen clearly from the figures of the difference between the predicted and observed temperature (Fig. 4.10d), and in the difference between their trends (Fig. 4.10f). This implies that the vertical velocity as estimated above is consistent with the thermal structure and horizontal advective heat fluxes for all depths except within the MLD during early NE monsoon. This result ensures that horizontal advective heat flux within the ML during the early NE monsoon is not correct.

4.2.2 Estimating the vertical velocity: case of Reynolds-based horizontal advection

The model is used to estimate the vertical velocity using the same method as used above, but now using Reynolds-based horizontal advection (section 3.2.5). The predicted vertical velocity for the case is presented in Fig. 4.11 (contour). The associated estimate of vertical advection of heat (colour) is also shown. The estimates of vertical velocity are large and structured during both NE monsoon and SW monsoon. Weak and episodic vertical movements are present during the inter-monsoons. Strong upwelling occurs during November (4 m day^{-1}), July (4 m day^{-1}), and second half of August (2 m day^{-1}). Strong downwelling occurs during December (4 m day^{-1}) and mid-August (4 m day^{-1}).

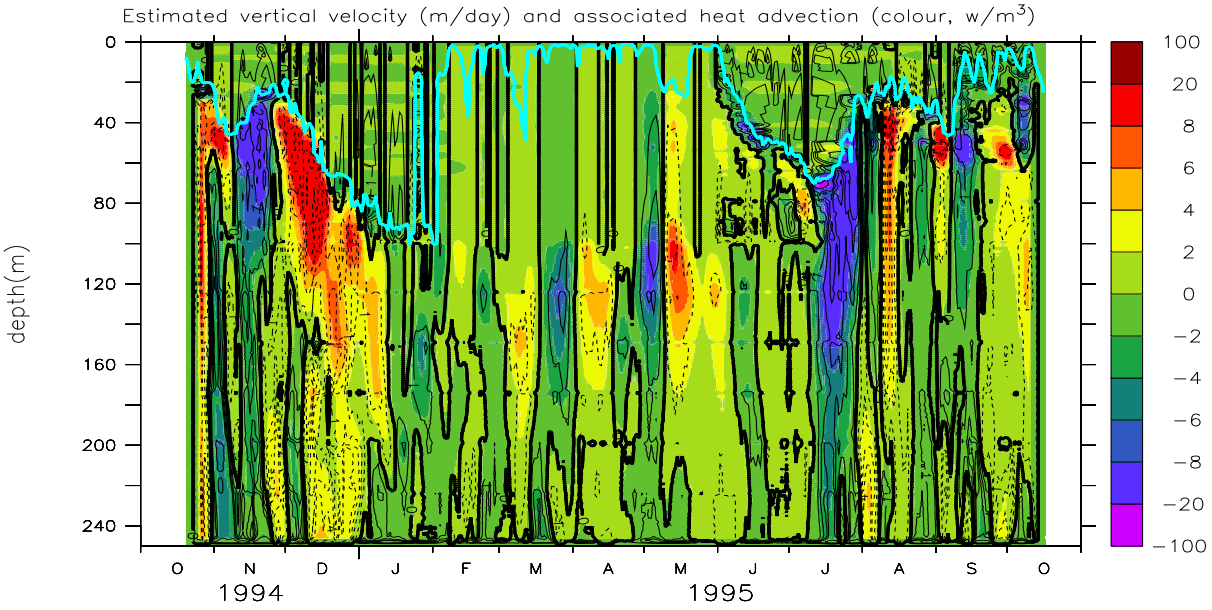

Figure 4.11: (a) Contours of vertical velocity (m/day) estimated in the present study: solid lines - negative velocities; dashed lines - negative velocities; thick solid lines - zero velocities. The contour intervals are 1 m day^{-1}. Associated estimates of advective heat fluxes (colour, W m^{-3}) are also shown together with MLD (blue line).

The estimated vertical velocity (WRR) at 100 m is averaged over two months and compared with SODA-based vertical velocity (WS) and Ekman pumping (WEk) velocity in Fig. 4.12 (as resolution of SODA vertical velocity is one month). All the estimates are comparable to each other and are of same phase during most of the year. They show downwelling during the NE monsoon and upwelling during the SW monsoon. The predicted estimates are relatively stronger (two times) than WS and WEk.

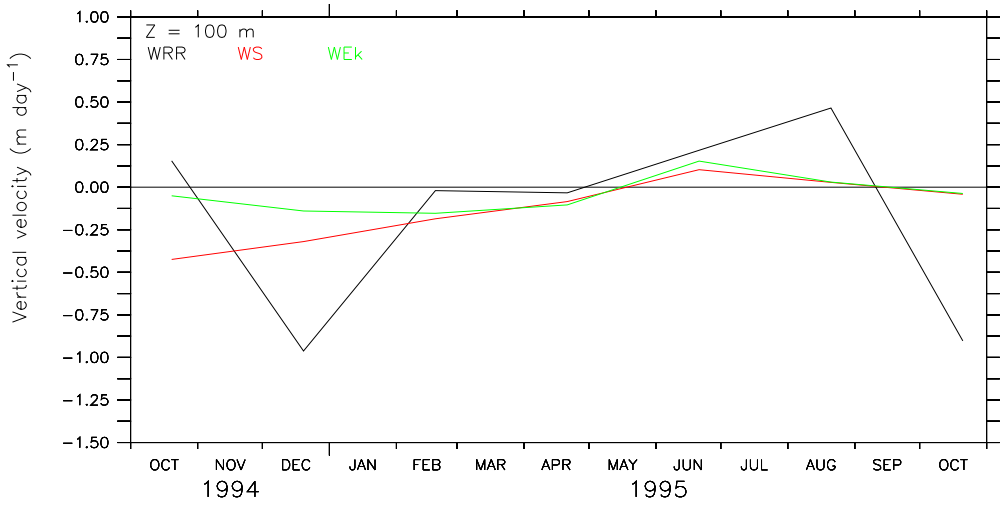

Figure 4.12: Predicted vertical velocity (WRR) at 100 m compares with the SODA-based vertical velocity (WS) and Ekman pumping velocity (WEk) based on ECMWF wind stress. The data are averaged over two months.

4.2.2.1 Testing WRR: Temperature simulation with atmospheric fluxes, Fischer-based horizontal advection, and WRR (S3c)

As we estimated vertical velocity, these estimates need to examined for their consistency. Therefore, simulation of temperature field is carried out by forcing the TKE model with the estimated vertical velocity (see Fig. 4.11) to include the effect of vertical advection together with the corresponding estimates of horizontal advective heat fluxes and local air-sea fluxes (as used in S3a). The prediction is expected to match the observations. The results of the simulation (S3c) are presented in Fig. 4.13. As shown, the thermal structure is reproduced well. The predicted SST (Fig. 4.13a) and MLD (4.13a) remains close to the observations all through the year. The observed intra-seasonal variations in temperature vertical structure are reproduced well (see Fig. 4.13c). The differences between the simulated and the observed temperatures remain small (within $\pm 1\,^{\circ}$C) at all depths (Fig. 4.13d). As regards temperature trend, all the cooling and warming trends in the sub-surface layers are reproduced well (Fig. 4.13e-f).

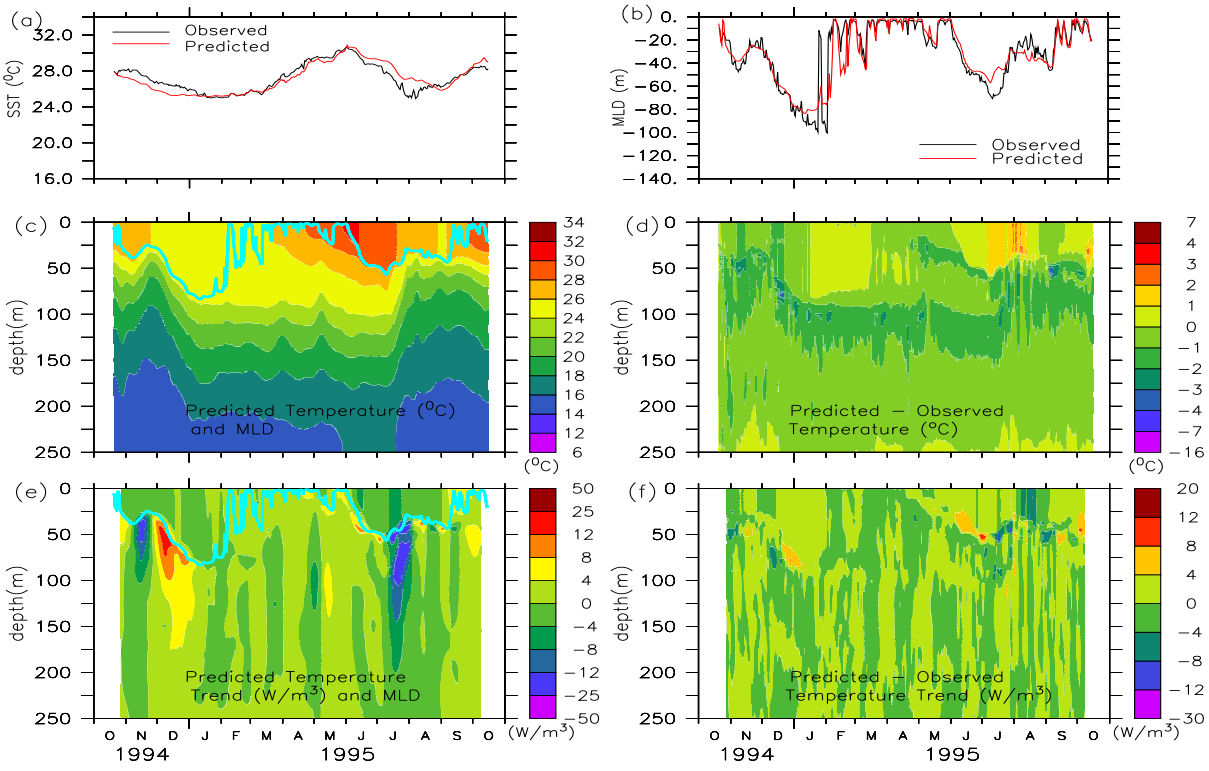

Figure 4.13: Results of the numerical simulation S3c: (a) predicted (red) and observed (black) SST; (b) predicted (red) and observed (black) MLD; (c) vertical structure of predicted temperature (color) and MLD (blue line); (d) modeled minus observed temperature; (e) vertical structure of predicted temperature trend (color) and MLD (blue line); (f) predicted minus observed temperature trend. The data are smoothed as in Fig. 4.1.

4.2.3 Comparison between the two predicted vertical velocities

A comparison between the two estimates of vertical velocity (WFR, corresponding to Fischer et al. [4] estimates of horizontal advection, and WRR, corresponding to horizontal advection based on Reynolds temperature gradient) is presented in Fig. 4.14. The velocities at 5 m below the ML and at 100 m are presented in Fig. 4.14a and Fig. 4.14b respectively. The average vertical velocity between the MLD and 125 m is presented in Fig. 4.14c. It can be seen that WFR differs significantly from WRR during the period when the first estimates of horizontal advective heat fluxes are associated with strong signals of warming and cooling events; else, both estimates are similar. The features common to both estimates are downwelling during mid-December to early January (3 m day^{-1}) and during mid-August (2 m day^{-1}), and upwelling during early May and late August (2 m day^{-1}). The downwelling is more pronounced in the deeper layers (at 100 m) and upwellings is more pronounced near the ML. Both estimates show weak vertical movement

during most of the inter-monsoons.

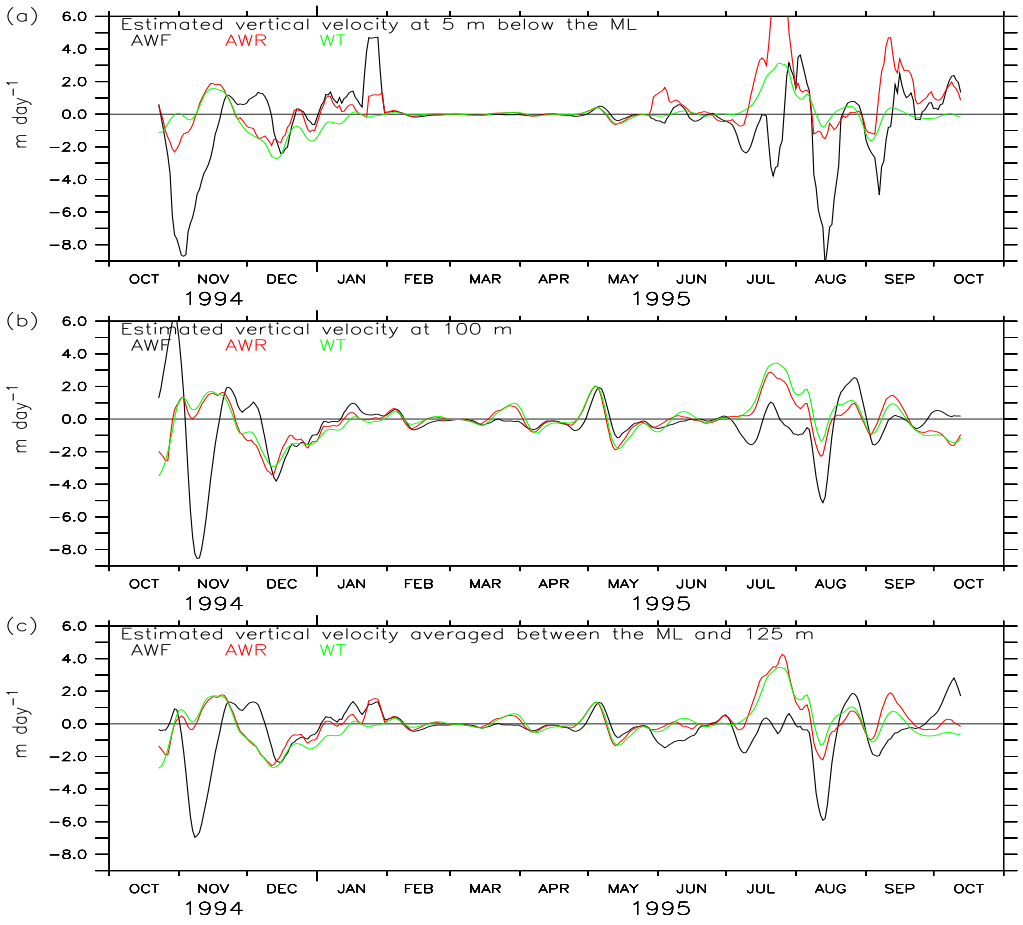

Figure 4.14: Comparison between the predicted estimates of vertical velocities (WFR: closure to the horizontal advective heat fluxes based on Fischer et al. [4] estimates; AWR: closure to the horizontal advective heat fluxes based on Reynold's T gradient) and vertical velocity estimated based on Isotherm excursion (WT). (a) Vertical velocity at 10 m below the ML (b) vertical velocity at 100 m, (c) velocity averaged between the ML and 125m.

It is worth analysing what process generates the estimated vertical velocity. For this, the vertical velocity due to Ekman pumping was computed using ECMWF winds and compared with the predicted vertical velocities WFR and WRR in Fig. 4.15. The comparison suggests that the strong vertical velocity during the NE monsoon does not depend on local wind stresses, implying that the velocities during this period are mostly driven by geostrophy. The vertical velocity during the SW monsoon is driven partly by local wind stresses and partly by geostrophy.

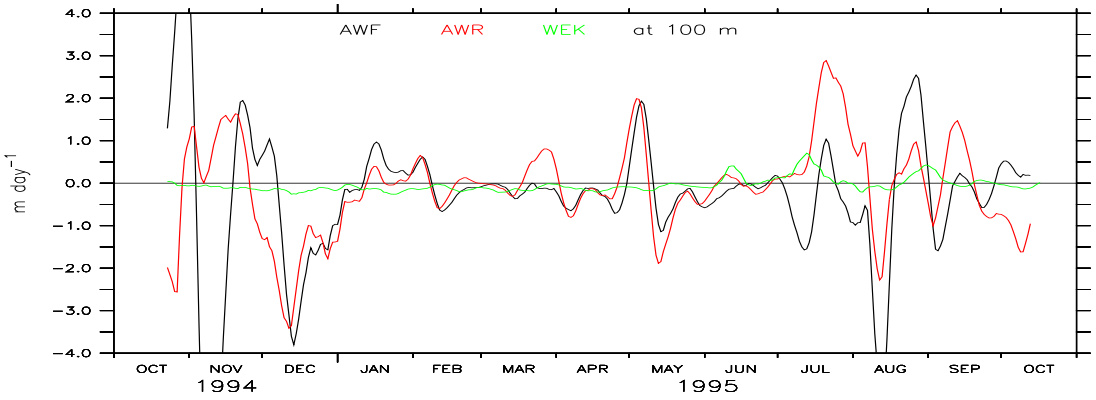

Figure 4.15: Comparison between the predicted vertical velocities at 100 m and Ekman pumping vertical velocity estimated using ECMWF winds at the study location.

4.2.4 Discussion

The method used to predict the vertical velocity helps in reproducing the vertical structure. The main limitation of the method is that it cannot predict the vertical velocity within the ML. The linear interpolation of the vertical velocity (between zero at surface and model predicted value at one level below the MLD) may not be appropriate. Imperfect temperature prediction in simulation S2c (section 4.2.1.1) is due to this interpolation.

The analysis (section 4.2.1.1) of simulation S2c leads us to question the enormous cooling present in Fischer et al.'s [4] estimate of horizontal advective heat fluxes within the ML during early NE monsoon (mid-October to mid-November). The simulation S2c* was carried out, similar to S2c, by assuming a zero value for the horizontal advective heat flux within the ML during early NE monsoon. The predicted temperature structure matches the observation throughout the year at all depths. This is an additional clue that Fischer et al. [4] estimates are wrong for this period. The excess cooling during the early NE in their estimate is an artifact.

Both the predicted vertical velocities WFR and WRR are dependent on the horizontal advective heat fluxes and atmospheric forcing fluxes and thus reflect the possible errors in these forcing fluxes. The atmospheric fluxes used in the model are accurate (hardly 2–3% error) (as implied in the sensitivity experiment carried out in section B.3). Fischer-based advective heat fluxes are associated with large uncertainties (Fischer et al. [4]). Reynolds-based horizontal advective heat fluxes may also contain large errors in the sub-surface (due to the assumption used to extrapolate the surface SST gradient). It is thus important to examine the sensitivity of the estimated WFR and

WRR to the horizontal advective heat fluxes. The results of simulations corresponding to a 50% increase and decrease in Fischer-based horizontal advective heat flux (see Fig. F.2a in Appendix F) show that the upwelling during late-November, during early May, and during late-August, and downwelling during December are not influenced by the change, whereas the downwelling during early November and during July–August are affected significantly by the changes (strength of downwelling during early November reduce from 7 m day^{-1}to 2 m day^{-1}, and downwelling during July–August becomes an upwelling if the Fischer-based flux is decreased by 50%). Similar experiments with the Reynolds-based flux suggest that the features in predicted vertical velocity (WRR) are not influenced by a 50% change (see Fig. F.2b in Appendix F).

Though the predicted vertical velocities WFR and WRR are derived using two different sources of horizontal advective heat fluxes, they agree in predicting significant downwelling during December (upto 3 m day^{-1}), relatively weak downwelling during May and August (upto 1.5 m day^{-1}), significant upwelling during late-November, early-May, and August (upto 2 m day^{-1}). These sensitivity analyses also suggest that upwelling could prevail during July to early August.

The WFR (corresponding to Fischer-based horizontal advection) is much weaker than the heat conserving vertical velocity W_H of Fischer et al. [4]. This leads us to question the method of their estimation. The WRR is stronger than the estimates of SODA-based vertical velocity, however, their seasonal evolution is in phase.

By assuming that the contributions of horizontal advection to the vertical movement of thermocline in the sub-surface layer is negligible, vertical velocity (WT) has been estimated from the observed temperature profiles using the technique presented in appendix E. These estimates of WT are mostly the same as the predicted vertical velocity corresponding to the Reynolds-based horizontal advective heat fluxes (see Fig. 4.14). The strength of WT is upto 4 m day^{-1}and the seasonal variability associated with this estimate is quite similar to SODA-based vertical velocity.

4.2.5 Concluding remarks

The analysis of predicted vertical velocity (WFR and WRR) suggests that during the NE monsoon and SW monsoon, vertical velocity is strong. There is downwelling during December and August and upwelling during July and late August. Vertical movement is weak during the inter-monsoons. This implies vertical advection is an important process in controlling the thermal structure during the monsoons.